Available online at www.sciencedirect.com
SCIENCE DIRECT
Polymer 47 (2006) 403–414
polymer
www.elsevier.com/locate/polymer

Molecular interactions in intercalated organically modified clay and clay–polycaprolactam nanocomposites: Experiments and modeling

Kalpana S. Katti *, Debashis Sikdar, Dinesh R. Katti, Pijush Ghosh, Devendra Verma

Department of Civil Engineering and Construction Management, North Dakota State University, Fargo, ND 58105, USA

Received 10 August 2005; received in revised form 15 November 2005; accepted 16 November 2005

Abstract

In this work we have evaluated molecular interactions in organically modified clay and polymer clay nanocomposite using a combination of experimental (photoacoustic FTIR, XRD) and computational (molecular dynamics (MD)) techniques. The FTIR data reveals hydrogen bond and ionic bond interaction between functional end groups of organic modifier and surface oxygen of interlayer clay sheet lying in the organically modified clay; and, the hydrogen bond formation between intercalated polymer and organic modifier and surface oxygen of clay sheet lying in the interlayer clay gallery in the polymer clay nanocomposite. In this work we report the nature of interactions between clay and polymer, clay and organic modifier in polymer–clay nanocomposites through experiments and molecular dynamics simulations.

Keywords: Clay nanocomposites; Fourier transform infrared spectroscopy; Molecular dynamics

1. Introduction

In recent years the polymer–clay nanocomposites (PCN) have drawn much attention of researchers because of significant improvement in mechanical properties [1–12], thermal properties [7,13–20], decreasing permeability [4,5,21], influencing biodegradability of biodegradable polymers for biomedical applications [22], etc. in comparison to polymers without nanoclay fillers. Most notable is the improvement in elastic modulus [4–6], increased tensile strength or elongation strain [7,9], decreased water/gas permeability [3–5], enhancement in thermal resistance and decrease in flammability [7–12]. Due to these properties, PCN have potential applications in the automobile, aviation, geotextile, biomedical and other polymer industries where the use of the polymers is abundant and property enhancement (mechanical, thermal, etc.) is the primary concern.

PCNs consist of nanosized clay particles dispersed in a polymer matrix. Processing of PCNs is done in several different ways. These include solution intercalation [10,11,21], in situ polymerization [19] and melt blending [7,8,20]. The nanocomposites thus formed are basically of two types: intercalated nanocomposite, in which the unit cells of clay structure are expanded by insertion of polymer into the interlayer spacing while the periodicity of clay crystal structure is maintained; and, other is exfoliated nanocomposite where the crystal structure of clay is completely delaminated by individual dispersion of clay layers into the polymer matrix.

For synthesis of PCNs, several polymers such as vinyl polymers, condensation polymers, polyolefins, specialty polymers and biodegradable polymers are used. The choice of clay is often one with layered silicate structure. Most commonly, montmorillonite (MMT) is used due to its highly expansive characteristic. The MMT unit cell is composed of aluminum octahedra sandwiched between two silica tetrahedra with the unit cell dimension of about 1 nm in thickness and lateral dimension ranging from 30 nm to several microns. An isomorphous substitution of Al^{+3} in the octahedral layer by Mg^{+2} or Fe^{+2}, or Mg^{+2} replaced by Li^{+1} imparts charge negativity to the MMT unit cell and attracts the positive cations like Na^{+1} or Ca^{+1} in the interlayer of clay gallery for charge balancing [23]. The water molecules in contact with MMT enter into the interlayer clay gallery and cluster around the interlayer cations like sodium, iron, magnesium etc. In the silica tetrahedra, partially charged oxygen atoms covalently bonded with silicon remain on the surface. The hydrogen of water molecules in the clay gallery bond with the surface oxygen in the clay gallery and thus result in the expansion of clay. This expansive nature of MMT is particularly utilized in making the PCN by inserting the polymer into the expanded

* Corresponding author. Tel.: +1 701 231 9504; fax: +1 701 231 6185.
E-mail address: kalpana.katti@ndsu.edu (K.S. Katti).

0032-3861/$ - see front matter © 2005 Elsevier Ltd. All rights reserved.
doi:10.1016/j.polymer.2005.11.055

interlayer spacing between clay unit cells. For facilitating better miscibility of hydrophobic polymer with clay and increasing the spacing of interlayer clay gallery, the clay is often treated with organic modifiers which are generally long carbon chain compounds with alkylammonium or alkylphosphonium cations [23].

The first PCN was developed by Toyota R&D labs in 1990 in Japan. Since then, considerable amount of work has been done on the synthesis, characterization and modeling of PCN. Recently, Chen et al. [24] synthesized a novel polyurethane–clay nanocomposite that is completely exfoliated by solution intercalation technique using Na^+-MMT clay and 12-aminolauric acid and benzidine as modifiers. In this PCN, 200% increase in tensile strength and 300% increase in elongation at break was obtained with respect to that of pure polymer. Also, Liang et al. [25] have reported organo modification of MMT by thermally stable aromatic amines, which contained thermally stable phenyl structure and unlike aliphatic amines which are chemically very rigid. The exfoliated polyimide–clay nanocomposites prepared through in situ polymerization technique have shown significant improvement in thermal stability and decrease in coefficient of thermal expansion. It was reported that the clay content in PCN has marked influence over the properties of nanocomposites. Recently, Ma et al. [11] have studied the effect of swelling agents on the crystallization behavior and mechanical properties of nylon6-clay nanocomposites. From the differential scanning calorimetry study they found that clay induced γ-form of crystals of PA6 in the PCN and clay acted as a nucleating agent that enhanced the crystallization rate of PA6. On the other hand, the PCN showed up to 143% increment in tensile and flexural strength. Several kinds of nylon11-clay nanocomposites containing different degrees of intercalated and exfoliated clays by melt compounding technique have been also prepared [15]. For clay content less than 4 wt%, an exfoliated PCN was obtained. The PCN exhibited 100% increment in storage modulus, and remarkable improvement in elastic and yield strength with respect to the pristine polymer. A novel synthesis procedure of exfoliated poly(styrene-*co*-methyl methacrylate)–clay nanocomposite has been proposed by Xu et al. [19] using emulsion polymerization technique. They studied the rheological, mechanical and thermal property of the PCN, which showed 20% improvement in thermal decomposition temperature and significant enhancement in dynamic storage modulus in comparison to pure polymer. The effect of phosphonium modifier of varying chain lengths on the properties of organoclays has shown that with the increase in chain length of modifiers, the miscibility of clay with the polymers and interlayer spacing of clay can be increased [4]. The effect of organic modification of clay and the effect of shear on the formation of polypropylene and polystyrene clay nano composites has also been investigated [7]. Further, the addition of small amounts of organoclay improves the mechanical properties and thermally stability of PCN significantly with respect to the pure polymer [21].

Although significant work has been done recently in the synthesis and fabrication of PCNs, the key mechanisms of intercalation behavior at clay-modifier-polymer interfaces are still not well understood. Fourier transform infrared spectroscopy (FTIR) is a very useful technique for studying molecular interactions, especially to uncover the interactions of the polymer, clay and organic modifier. Recently the hydrogen bonding characteristics of interaction between silicate layers and polyamide6 (PA6) and nature of hydrogen bonding and different crystalline phases in PA6 has been studied with transmission FTIR [26]. It has been shown that the presence of silicate layers weakens the hydrogen bonding in both α and γ phases of PA6 and although PA6 is most stable in α-phase, the addition of clay silicate layers favor the γ phase of PA6 crystals. Jong et al. [27] used FTIR transmission experiments to examine the effect of pretreatment of cation exchanged MMT samples at different temperatures in order to investigate the influence of adsorbed water and hydroxyl groups in the bonding mechanism and interaction behavior of alkyl ketones with MMT surface. Further, Jong et al. [28] studied the nature of adsorption of acetylacetone on the surface of clay. After treating MMT with acetylacetone, the C=O band shifts to lower energy. It is postulated that this may be due to chemical interaction of C=O with structural hydroxyl of montmorillonite or linking of acetylacetone to an exchangeable metal cation of montmorillonite through a water bridge or cationic hydroxyl group. The modification effect of MMT by alkyl ammonium is studied using transmission FTIR [29]. A new band at 1667 cm^{-1} in the nanocomposite was found, which was assigned to C=C stretching vibration which indicates the formation of double bonds in the composite. Polymorphism in nylon-11/MMT nanocomposite was observed using transmission FTIR [30]. Mingkui et al. [31] conducted studies on poly(vinyldine fluoride-hexafluoropropylene)-MMT nanocomposite through transmission FTIR and reported the formation of nanoscale micro environment in the silicate and attributed some band shifting in PCN for the increase in ionic interaction in the materials after formation of nanocomposites.

Thus, it is understood that the modification of clay by organic modifier increases the interlayer spacing of clay and creates more conducive thermodynamic energy state in the clay gallery to interact the hydrophobic polymer with the clay. Yet the interactions of the clay with organic modifier in organically modified clay and the interactions of clay, polymer and organic modifier in PCN are not clearly understood. Recently, some molecular modeling efforts have also been attempted to model the clay interlayer [32–41]. By molecular modeling, Tanaka et al. [42] studied the PCN containing nylon6,6 as polymer and exfoliated clay layers treated with twelve different organic modifiers and found that binding energy between clay and polymer is highest and it diminishes linearly as the volume of intercalated organic modifier in clay increases. In the investigation of behavior and morphology of nanoconfined quaternary alkylammoniums in organically modified clay, Zeng et al. [43] conducted molecular dynamics simulation over the OMMT models containing two clay layers and different quaternary alkylammoniums. Their observation exhibits that intercalated alkylammoniums with in silicate sheets take layer conformation. The end groups of long alkyl ammonium chains

remain close to the clay surface, however, the orientation of backbone chain depends on the charges of the atoms of clay surface as well as the backbone chain length of the surfactants. Minisini et al. [44] using molecular mechanics studied the influence of chemical structures of surfactant on the expansion of basal spacing and the electrostatic potential bonding between two clay layers in OMMT.

Using MD, Shah et al. [45] investigated the process of change of shape of surfactants in the water–silica interfaces. Their study revealed that the surfactant (*n*-dodecyltrimethylammonium bromide) takes spherical or elliptical shape in the aqueous solution, which changes into flat elliptical shape at the hydrophobic silica surface. In a separate morphological investigation of organically modified clay by molecular dynamics, Zeng et al. [46] studied the behavior of organically modified clay treated with dioctadecyldimethylammoniums. They compared their MD results with the experimentally observed results of XRD, atomic force microscopy (AFM), FTIR and neutron magnetic resonance (NMR) spectroscopy and found a good agreement between the modeling and experimental results. Their observation shows that the nitrogen atoms of surfactants always lie within the interlayer clay galleries. The backbone chain of intercalated organic modifiers prefer the parallel orientation with respect to interlayer clay surface whereas the organic modifiers outside the clay gallery prefer orientation perpendicular to clay surfaces. Although the methylene chain of organic modifiers show the ordered orientation in and outside the organically modified clay but the functional groups show the random orientation in both the cases. The organic modifiers within the clay gallery show both the trans and gauche conformations although the trans conformation is dominant. Hackett et al. [47] studied the static and dynamic properties of layer silicates treated with alkylammonium surfactants using molecular dynamics. They noticed that organic and inorganic layers assemble each other in alternate layers in well ordered manners to form the organically modified clay.

Unless the bond mechanism and nature of molecular interactions are completely understood, good control over the properties of the PCN cannot be obtained. In this study, we have investigated the mechanism of bonding and interactions of polymer, clay and organic modifier in polymer–clay nanocomposites using experiments and molecular dynamics simulations.

2. Materials and methods

2.1. Materials

Na-Montmorillonite (Swy-2, Crook County, Wyoming, USA) of cationic exchange capacity 76.4 mequiv/100 mg was obtained from the Clay Minerals Repository at the University of Missouri, Columbia, MO, USA. 12-Aminolauric acid [$NH_2(CH_2)_{11}COOH$] was obtained from TCI America. Polyamide6 (PA6) [$(CH_2)_5CONH]_n$ of molecular weight 16,000 was obtained from Polysciences, Inc, USA. Formic acid (97%), methanol anhydrous (99.9%), silver nitrate, acculute standard volumetric solution, final concentration 0.1 and 0.1 N hydrochloric acid [HCl] were purchased from Alfa Aesar, MA, USA.

2.2. Preparation of organically modified montmorillonite (OMMT)

Sodium montmorillonite (Na-MMT) was crushed into fine powder and screened through #325 sieve (45 μm). Ten grams of this Na-MMT sample was completely dispersed into 200 ml of water which was preheated to 333 K. Further 3.312 g (15.4 mmol) of 12-aminolauric acid and 2.5 ml of 0.1 N HCl were added to 800 ml of deionized (DI) water at temperature, 333 K and stirred to make a uniform solution. In this solution, the clay suspension was gradually added and finally, the resulting solution was stirred vigorously at 333 K for 1 h. The modified montmorillonite was washed several times with DI water until the Cl^- was completely removed from the clay. The filtrate was titrated with the 0.1 N $AgNO_3$ until no AgCl was further formed which indicated the complete removal of Cl^- from the OMMT. Finally, the OMMT cake was placed in the oven at 353 K for 24 h and the dried OMMT was ground and passed through 325-mesh sieve for synthesis of PCN.

2.3. Synthesis of polymer clay nanocomposite (PCN)

Ten grams of PA6 was added with 155.73 ml (190 g) of formic acid (FA) and stirred vigorously for 40 min to make the uniform solution. Two weight percents of OMMT (5, 9 wt% of OMMT with respect to pure PA6) were added to the PA6-FA solution and stirred vigorously for 6 h. The resulting PCN was obtained in the fibrous form. It was washed several times with DI water to remove the FA completely from the PCN and then washed with the methanol to remove the water from the fibrous PCN. It was then dried in the vacuum dessicator at 313 K temperature for 24 h to remove the water completely and finally the PCN was obtained. The synthesis of OMMT and PCN was based on procedures by Ma et al. [11].

2.4. Modeling and simulation

We used molecular dynamics to study interactions between clay and organic modifier. The simulation of the organically modified clay model was then carried out using molecular dynamics software NAMD, version 2.5 by Theoretical Biophysics Group, University of Illinois and Beckman Institute, Urbana, IL, USA. VMD, version 1.8 of Theoretical Biophysics Group, University of Illinois and Beckman Institute, Urbana, IL, USA was used for all interactive studies. The force field used for simulation was CHARMm. In our previous work, we have derived the Na-MMT clay parameters for CHARMm force field taking the clay parameters from CFF force field to study the interactions of clay–water system [32–34]. In the present study, these previously determined Na-MMT parameters have been used to study the interactions of Na-MMT and organic modifier for the OMMT system. The simulation was done at the Center for High Performance

Computing (CHPC) at North Dakota State University, USA. The simulations were conducted on parallel computers with 96 nodes (DakTech nodes)/192 processors (three Gigahertz Intel/XEON processors). First ion substituted MMT and the modifier, 12-aminolauric acid were modeled individually using Accelrys group software, InsightII (2000) using module Builder™. The starting structure used in this simulation has unit cell dimension $x=5.28$ Å, $y=9.14$ Å, and $z=6.56$ Å. In the case of MMT, 4X2-unit cell model was constructed containing four unit cells in the x direction and two unit cells in the y direction. The resultant dimension of the clay model was 21.12 Å×18.28 Å×6.56 Å. The coordinates of the clay unit cells are based on those given by Skipper, Chang and Sposito [48,49]. Ion substituted MMT model was obtained substituting Al^{3+} ions from the aluminum octahedral layer with either Fe^{2+} or Mg^{2+} in alternate clay units. Four strands of 12-aminolauric acid were placed horizontally into the interlayer clay gallery of montmorillonite with respect to clay surface. Initial models of dry MMT and OMMT are shown in Fig. 1.

The model was equilibrated at zero pressure and at a temperature of 0 K to minimize the initial constraint energy involved in the model. Further, the temperature was raised to 300 K for dry MMT model, using Langevin method. Increment in temperature was followed by rise in pressure to 1 atm in four steps. For OMMT model, the temperature was further raised to 333 K and then again lowered to the 300 K under 1 atm pressure to simulate the experimental processing condition. For MMT and OMMT models, energy minimization followed by molecular dynamics simulation with temperature and pressure was run for sufficiently long time of 25 ps (10^{-12} s) and 100 ps, respectively, to ensure the convergence of energy. The time step used for the simulation was 0.5 fs (10^{-15} s). All the simulations were performed under NPT ensemble (constant number of particles, pressure and temperature). Periodic boundary conditions for simulation of MMT model were maintained 27, 24, and 25 in x, y, and z directions, respectively, and those for OMMT model were set 27, 24, and 35.20 in x, y, and z directions respectively. Cut-off distance of 12 Å was used for both the models for calculation of van der Waals forces. Particle Mesh Ewald (PME) technique was used for the calculation of electrostatic forces.

2.5. Characterization

2.5.1. XRD characterization

The X-ray analysis was done using X-ray diffractometer (model Philips X'pert, Almelo, Netherlands) equipped with secondary monochromator and Cu-tube using CuKα radiation of wavelength 1.54056 Å. The d-spacing of clay structure was calculated from the XRD data. For MMT and OMMT, the clay was finely crushed and screened with 45 μm sieve and then wide angle X-ray diffraction was done at a scan rate of 2°/min in each case and scan range of $2\theta=2.01$–65° for MMT and $2\theta=2.01$–35° for OMMT. The fibrous PCN was compressed into thin sheets using a mechanical testing device, SATEC (model 22 EMF, PA, USA) under the compressive stress of 40 MPa maintained for a duration of 10 min. The X-ray diffraction was done at a scan rate of 4°/min and for the range of $2\theta=2.01$–15°.

2.5.2. Photoacoustic (PA) FTIR characterization

PA FTIR technique can be used in the study and characterization of absorbed and chemisorbed molecular species and compounds on the surface of metals, semiconductors, and even insulator [50]. PA FTIR experiments were conducted in FTIR bench (model Nexus, Thermo Nicolet, USA) using a photoacoustic cell (MTEC Photoacoustics model no. 300). Linear photoacoustic experiments were conducted for 500 scans at a resolution of 4 cm^{-1}. DTGS detector with KBR beam splitter was used for data acquisition. Powder sample of pure MMT, OMMT, organic modifier and fibrous PCN sample were pressed into pellets using the mechanical testing device SATEC (model 22 EMF, PA, USA) at the compressive stress of 15 MPa and for the duration of 10 min. The PA6 sample was heated gradually from 303 to 493 K and then pressed similarly into pellets. The PA FTIR was done in each case in the linear photoacoustic mode with moving mirror velocity of 0.1581 cm/s. The data were acquired for the wavenumber range of 4000–400 cm^{-1}.

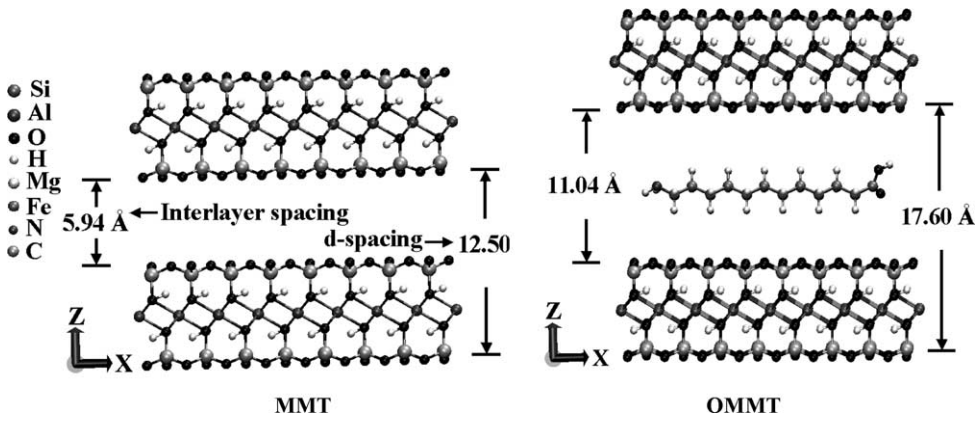

Fig. 1. Initial structure of MMT and OMMT before minimization.

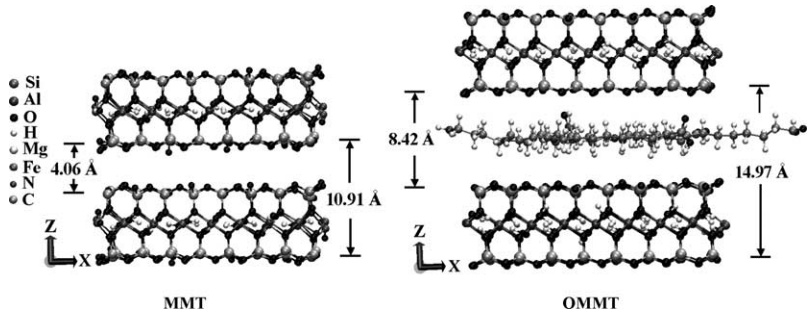

Fig. 2. Structure of MMT and OMMT at 300 K temperature and 1 atm pressure.

3. Results and discussion

3.1. Simulation results

From Fig. 1 it is seen that the d_{001} spacing and interlayer clay-gallery height of MMT before simulation are 12.50 and 5.94 Å and those for OMMT are 17.60 and 11.04 Å, respectively. The final form of NPT simulation of MMT and OMMT are shown in the Fig. 2.

It is observed that the d_{001} spacing and interlayer clay spacing of MMT are 10.91 and 4.06 Å, respectively, and those for the OMMT are 14.97 and 8.42 Å, respectively. The shortest distance between the hydrogen atom of 12-aminolauric acid and the surface oxygen lying in silica tetrahedra of MMT was found to be 3.15 Å. The NPT simulated length of 12-aminolauric acid strand reduces to an average length of 10.93 Å from the pre-simulation length of 17.47 Å. The orientation of the 12-aminolauric acid is also changed from vertical to almost horizontal, with all the hydrogen atoms and end groups pointing towards the interlayer surface of clay sheet.

3.2. XRD results

The XRD scan of MMT, OMMT using organic modifier 12-aminolauric acid and PCN with 5 and 9 wt% OMMT loading with respect to pure PA6 are shown in the Fig. 3.

The peak corresponding to d_{001} plane of pure sample of MMT appears at $2\theta = 7.95°$. At this value of 2θ, the d_{001} spacing is 11.11 Å. In OMMT, the peak appears at $2\theta = 5.66°$, which corresponds to d_{001} spacing of 15.60 Å. The 4.49 Å increase in d_{001} spacing in the OMMT as compared to pure clay shows that the structure has intercalated. In the 5 and 9 clay% PCN, the peaks corresponding to d_{001} plane were observed at $2\theta = 6.59$ and 6.51°, respectively, and the corresponding d_{001} spacings were 13.40 and 13.49 Å, respectively. Although the d_{001} spacing of nanocomposites shows a slight decrease with respect to OMMT yet it is larger than that of clay, indicating an intercalated structure.

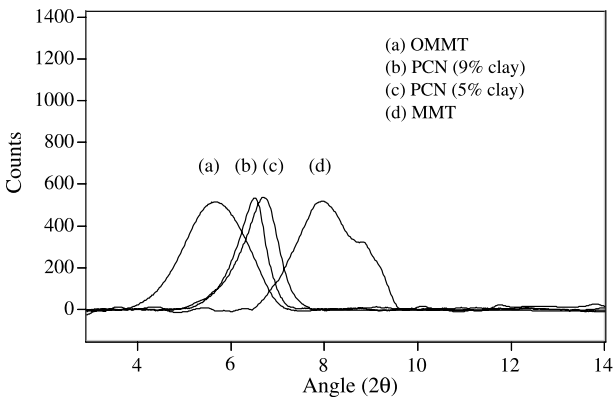

Fig. 3. X-ray diffraction data of OMMT, PCN and MMT.

3.3. FTIR results of Na^+-MMT, 12-aminolauric acid and OMMT

In Fig. 4, the FTIR data of pure MMT, 12-aminolauric acid (organic modifier) and OMMT are given.

Table 1 indicates the band assignments of all bands seen in Fig. 4. As seen in Fig. 4 from data on montmorillonite, the 400–3700 cm^{-1} region of the spectrum shows characteristic bands for O–H, Si–O as well as Al–O, Al–OH, AlFeOH, AlMgOH vibrations. Si–O deformations and Al–O/Si–O coupled bands as well as other bands are observed below 800 cm^{-1} as indicated in Table 1.

Also seen in Fig. 4 from spectrum of 12-aminolauric acid, characteristic bands of CH, N–H, O–H and C–N are observed. Also seen is a broad band in the region of 3182–2373 cm^{-1}, which is overtone of strong O–H stretching and weaker C–H

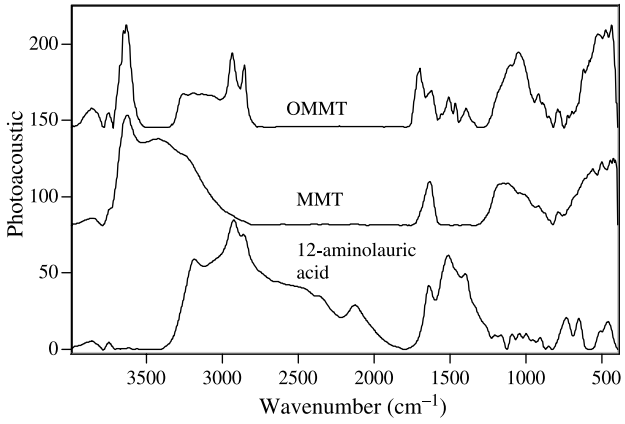

Fig. 4. Photoacoustic FTIR spectra of OMMT, MMT and 12-aminolauric acid in the energy range of 4000–400 cm^{-1} at scan speed of 0.15 cm^{-1}.

Table 1
Band assignments of photoacoustic FTIR spectra of montmorillonite (MMT), 12-aminolauric acid and organically modified montmorillonite (OMMT)

Sample	Wave number range (cm^{-1})	Bands	Refs.
MMT			
	3623	O–H stretching of structural hydroxyl group	[12,25,27,28,51–56]
	3234–3486	H–OH hydrogen bonded water	
	1635	O–H deformation of entrapped water	
	1110	Si–O in-plane stretching	
	1093	Si–O out-of-plane stretching	
	1045, 1025, 991	Si–O in-plane stretching	
	956	Si–OH vibrations	
	916	Al–O/Al–OH stretching vibration	
	883	Al–FeOH deformation	
	846	Al–MgOH deformation	
	796	Si–O stretching of quartz and silica	
	722	Si–O deformation perpendicular to optical axis	
	692	Si–O deformation parallel to optical axis	
	615	Coupled Al–O and Si–O out-of-plane vibration	
	562	Al–OSi deformation	
	449	Si–OFe vibration	
	428	Mg–O vibration	
12-aminola uric acid			
	3182	N–H stretching	[29,57–59]
	2922	C–H asymmetric stretching	
	2858	C–H symmetric stretching	
	2127	COO^- absorption and N–H stretching	
	1638	O–H bending and N–H deformation	
	1514	Asymmetric R–COO^- stretching	
	1403	Symmetric R–COO^- stretching	
	1206	Overlap of C–C stretching and CH_2 twisting	
	1163	CH_3 rocking	
	1094	C–N stretching	
	1045–957	CH_2 rocking and skeletonic stretching	
	909	C–H bending out of plane	
	853	C–C Skeletonic stretching	
	735	CH_2 rocking	
	655	N–H out of plane wagging	
	518–464	C–C bending	
OMMT			
	3646–3628	O–H stretching of structural hydroxyl group	[12,25,27–29,51–60]
	3256–3035	Ionic bonded N–H stretching	
	2932	C–H asymmetric stretching	
	2853	C–H symmetric stretching	
	1713–1701	C=O stretching	
	1623	Combination of O–H deformation and N–H bending	
	1511	Asymmetric R– COO^- stretching	
	1466	CO–H bending	
	1396	Symmetric R–COO^- stretching	
	1112	Si–O in-plane stretching	
	1060	Si–O in-plane stretching	
	1022, 997	Si–O in-plane stretching	
	963	Si–OH vibration	
	921	Al–AlOH deformation	
	884	Al–FeOH deformation	
	847	Al–MgOH deformation	
	799	Si–O stretching of quartz and silica	
	727	Si–O deformation perpendicular to optical axis	
	699	Si–O deformation parallel to optical axis	
	623	Coupled Al–O and Si–O out of plane	
	531	Al–OSi deformation	
	478	Si–OSi deformation	

stretching band. Other two combinations of bonds obtained in aminolauric acid are COO^- absorption band and N–H stretching band at 2127 cm^{-1}, and O–H bending and N–H deformation band at 1638 cm^{-1}. Also seen are strong absorption bands of R–COO^- group for asymmetric stretching and symmetric stretching are obtained in 1514 and 1403 cm^{-1}.

Further from Fig. 4, the IR spectrum of OMMT show features that are combination of characteristic bands of pure

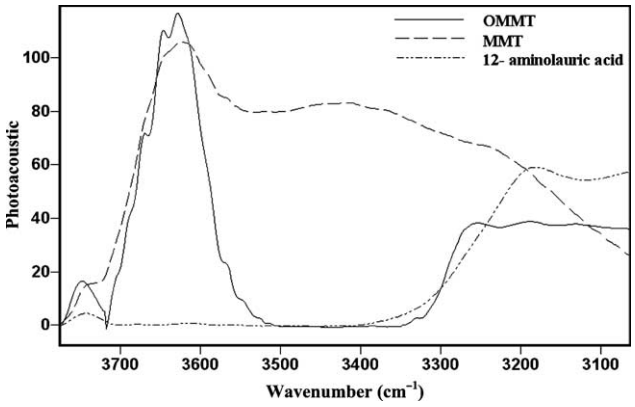

Fig. 5. Photoacoustic FTIR spectra of OMMT, MMT and 12-aminolauric acid in the energy range of 3800–3050 cm^{-1} at scan speed of 0.15 cm^{-1}.

MMT and 12-aminolauric acid. The broad band in the region of 3256–3035 cm^{-1} is assigned to ionic bonded N–H stretching band. The combination of O–H deformation and N–H stretching is assigned to 1628 cm^{-1}. The new bands at 1713 and 1701 cm^{-1} are attributed to C=O stretching. The bands coming after Si–O bands are primarily from interionic/non-bonded interactions of montmorillonite.

The PA-FTIR spectra of Na^+-MMT, OMMT and 12-aminolauric acid in the energy range of 3700–3100 cm^{-1} are shown in Fig. 5. A broad band at 3234–3486 cm^{-1} is found in Na^+-MMT, which is not present in OMMT. From the figure it is seen that the shape and position of N–H stretching band in OMMT has turned into wide band stretched over a long range of 3256–3035 cm^{-1} from a relatively sharp band in 12-aminolauric acid located at 3182 cm^{-1}.

Fig. 6 shows the PA FTIR spectra of Na^+-MMT, OMMT and 12-aminolauric acid in the range of 3200–2000 cm^{-1}. The shift of C–H asymmetric stretching band in OMMT by 10 cm^{-1} to higher energy is observed with respect to its position in 12-aminolauric acid. Similarly, the shift in the symmetric C–H stretching band by 5 cm^{-1} is found in OMMT in lower energy side with respect to its position in 12-aminolauric acid.

The PA FTIR spectra of Na^+-MMT, OMMT and 12-aminolauric acid in the energy range of 1800–1200 cm^{-1} are shown in Fig. 7. As seen, a new band appears in OMMT at

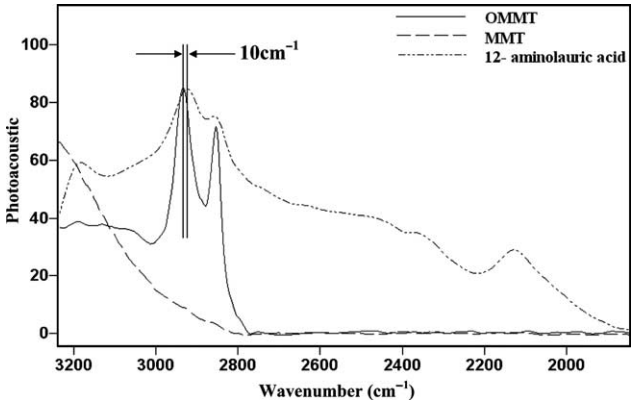

Fig. 6. Photoacoustic FTIR spectra of OMMT, MMT and 12-aminolauric acid in the energy range of 3250–1900 cm^{-1} at scan speed of 0.15 cm^{-1}.

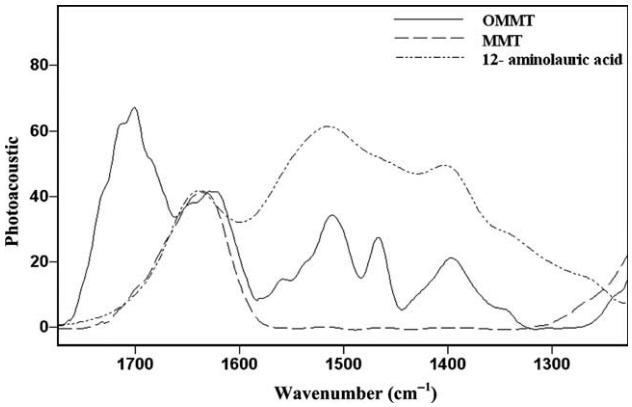

Fig. 7. Photoacoustic FTIR spectra of OMMT, MMT and 12-aminolauric acid in the energy range of 1800–1200 cm^{-1} at scan speed of 0.15 cm^{-1}.

1713–1701 cm^{-1}, which was not present in either MMT or pure 12-aminolauric acid. The band corresponds to the combination of N–H bending and O–H deformation has shifted to the lower energy side in OMMT by 16 cm^{-1} with respect to its position in pure 12-aminolauric acid. The band of O–H bending in OMMT has shifted to the lower energy side by 12 cm^{-1} with respect to its position in pure MMT. The R–COO^- asymmetric and symmetric stretching band at 1514 and 1402 cm^{-1} in 12-aminolauric acid are also present in OMMT at almost same positions but with the evolvement of new CO–H band at 1466 cm^{-1}. The primary difference of R–COO^- stretching bands in 12-aminolauric acid and OMMT is that in prior case these bands are much broader than those of OMMT.

The PA FTIR spectra of Na^+-MMT, OMMT and 12-aminolauric acid are shown in Fig. 8 for the energy range of 1250–800 cm^{-1}. The Si–O band in pure Na^+-MMT is much broader. The deconvoluted spectra of Si–O region of OMMT and MMT in the energy range of 1250–750 cm^{-1} are shown in the Fig. 9. It is seen that the in-plane stretching band in OMMT has shifted by an amount of 15 cm^{-1} to higher energy side with respect to its position (1045 cm^{-1}) in MMT. Si–O out-of-plane stretching band occurs in MMT at 1093 cm^{-1}, which completely disappears in OMMT.

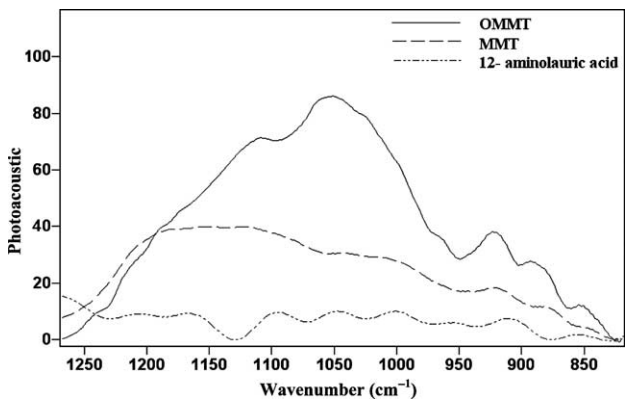

Fig. 8. Photoacoustic FTIR spectra of OMMT, MMT and 12-aminolauric acid in the energy range of 1300–800 cm^{-1} at scan speed of 0.15 cm^{-1}.

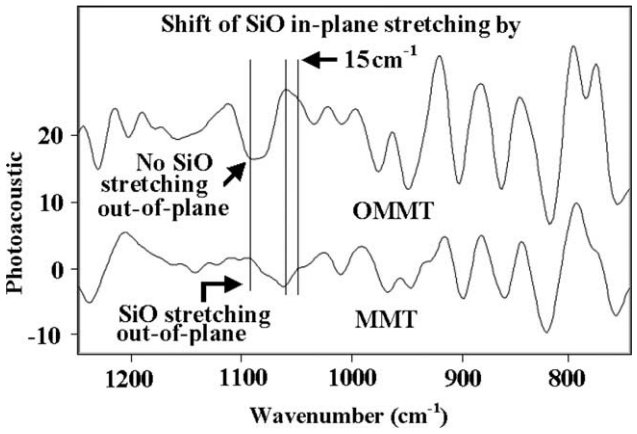

Fig. 9. Double derivative of photoacoustic FTIR spectra of OMMT and MMT in the energy range of 1300–750 cm^{-1} at scan speed of 0.15 cm^{-1}.

3.3.1. Discussion of FTIR results of Na^+-MMT, 12-Aminolauric acid and OMMT

In our sample, the COOH group of 12-aminolauric acid remains in dissociated form ($R–COO^-$) and therefore the $R–COO^-$ bands are obtained in FTIR spectrum of pure 12-aminolauric acid at the 1514 cm^{-1} and 1402 cm^{-1} for asymmetric and symmetric stretching respectively. During the synthesis of OMMT, when hydrochloric acid is added to the solution of DI water, 12-aminolauric acid and Na-MMT, the COO^- group and NH_2 of most part of 12-aminolauric acid is first protonated by H^+ of hydrochloric acid into COOH and N^+H_3 respectively. The H^+ of COOH is prone to form a hydrogen bond with the lone pair of surface oxygen of silicon tetrahedra lying in montmorillonite unit cell. This hydrogen bonded COOH group of 12-aminolauric acid appears to cause the evolvement of carbonyl band (C=O), O–H and hydrogen bonded C–O, which is seen in the spectra presented in Fig. 7. The carbonyl band (C=O) occurs in OMMT at 1713 and 1701 cm^{-1} and hydrogen bonded C–O band appears in OMMT at 1466 cm^{-1}, neither of which were present in pure 12-aminolauric acid. The appearance of new carbonyl bands in OMMT indicated that the organic modifier, 12-aminolauric acid in OMMT remains primarily in the protonated form. The residual dissociated COO^- groups of 12-aminolauric acid, which remains unreacted by H^+ of hydrochloric acid, produce the $R–COO^-$ bands in OMMT almost at the identical energy range as in 12-aminolauric acid. Because of reduction in concentration of $R–COO^-$ functional group in intercalated 12-aminolauric acid with respect to pure 12-aminolauric acid, the $R–COO^-$ bands should be comparatively sharper in OMMT, which is also evidenced in the spectra of OMMT presented in Fig. 8.

On the other hand, the N^+H_3 group of 12-aminolauric acid can cause ionic interaction with the lone pair of surface oxygen of silicon tetrahedra like $R^+–COO^-$ group. Because of the formation of ionic interaction between surface oxygen of montmorillonite and N^+H_3 functional group of 12-aminolauric acid, a broad N–H band is obtained in OMMT which is in perfect agreement with Fig. 5 where OMMT shows broad ionic bonded N–H stretching band in the range of 3256–3035 cm^{-1}, and the pure 12-aminolauric acid exhibits only the distinct N–H band at 3182 cm^{-1}. This ionic bond formation also causes the shifting of combination of N–H and O–H band in OMMT with respect to pure 12-aminolauric acid, which is also in agreement with spectra shown in Fig. 7.

The free water in the interlayer clay gallery of pure dry montmorillonite is replaced by organic modifier during synthesis of organically modified clay. This phenomenon is also apparent in the spectra. Fig. 5 shows that the dry montmorillonite has the broad band of H–OH stretching of water in the energy region of 3234–3486 cm^{-1}, which completely disappears in OMMT, indicating the interlayer water in OMMT is replaced by 12-aminolauric acid.

Because of the hydrogen bond and ionic bond formation between surface oxygen of silicon tetrahedra and functional end groups of 12-aminolauric acid, the energy of vibration in Si–O bond changes; which is also manifested in spectra. In Fig. 9 it is seen that the Si–O in-plane asymmetric stretching band in OMMT has shifted towards higher energy by 15 cm^{-1} from its position in pure montmorillonite. In Fig. 6, it is seen that the C–H stretching vibrations in OMMT have also shifted by 10 cm^{-1} to higher energy with respect to its position in pure 12-aminolauric acid. However, 12-aminolauric acid has a carbon chain containing 12 carbon atoms in its backbone chain. The shift in the C–H vibration is thus attributed to a combination of conformational changes in the molecule on entering the clay gallery and the tethering of end functional groups of organic modifier with surface oxygen in silicon tetrahedra.

In OMMT, the band corresponding to Si–O out-of-plane band is absent. This band is very prominent in MMT. One plausible explanation for it is that the organic modifier present in the interlayer clay gallery of OMMT has changed the orientation of tetrahedra–octahedra–tetrahedra (T–O–T) crystal structure of MMT in such a way that the unpolarized IR beam can no longer cause vibration of Si–O bond in out-of-plane mode and as a result of which no band resembling Si–O out-of-plane stretching vibration is found in OMMT. The change in MMT crystal structure for the presence of organic modifier can be established more firmly by doing the FTIR study of OMMT using polarized IR beam as IR light source.

3.3.2. Discussion of molecular dynamics simulation and XRD results of OMMT

From the simulation data, the d_{001}-spacing of OMMT is found to be 14.97 Å, which is very close to the experimentally obtained d_{001}-spacing, 15.60 Å obtained using XRD. Furthermore, from the simulation of OMMT structure it is seen that all the organic modifier molecules are oriented parallel to the interlayer clay surface and both the end groups (N^+H_3 and COOH) of organic modifiers are pointed towards the clay surface as shown in Fig. 10.

This indicates the tendency of end functional groups of organic modifiers of creating non-bonded interactions with the surface oxygen of interlayer clay sheets. Furthermore, the FTIR data of intercalated OMMT shows that H^+ of COOH and N^+H_3 end functional groups of organic modifier,

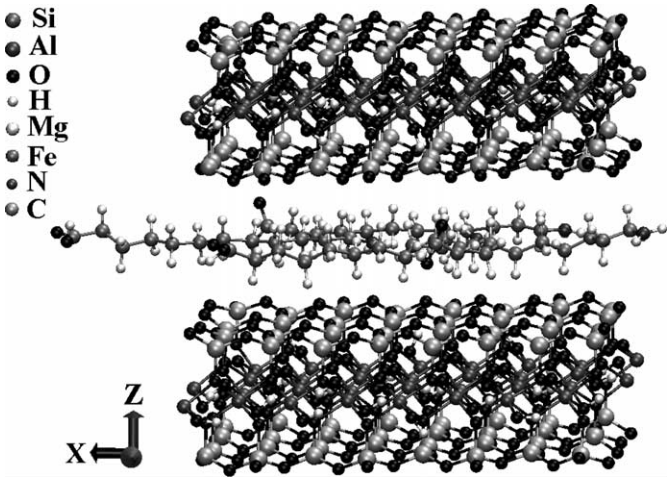

Fig. 10. Orientation of organic modifiers in the interlayer spacing of OMMT at 300 K temperature and 1 atm pressure.

12-aminolauric acid create hydrogen bond and ionic interactions respectively with the surface oxygen of interlayer clay sheets. Thus the simulation results combined with FTIR data predict that in OMMT, the orientation of organic modifier is parallel to the interlayer clay surface and the end functional groups of organic modifiers are creating hydrogen bond or ionic interaction with the oxygen lying on the interlayer silica tetrahedra surface.

3.4. FTIR results of polyamide 6 (PA6), OMMT and PCN

In Fig. 11, the PA FTIR spectra of OMMT, PA6 and PCN are shown. Band assignments of the bands in the 400–3900 cm^{-1} region are shown in Table 2.

As indicated in Table 2 we see characteristic bands from N–H, C–H, amide I, amide II as well as skeletonic C–C vibrations in this region.

In PCN, the band contribution from PA6 is much more prominent than that of OMMT. As indicated in Table 2 and from Fig. 11, the IR spectrum in PCN has bands from N–H, C–H, Si–O as well as CO–NH vibrations. The bands at lower energy range of 959–799 cm^{-1} are assigned to vibrations of

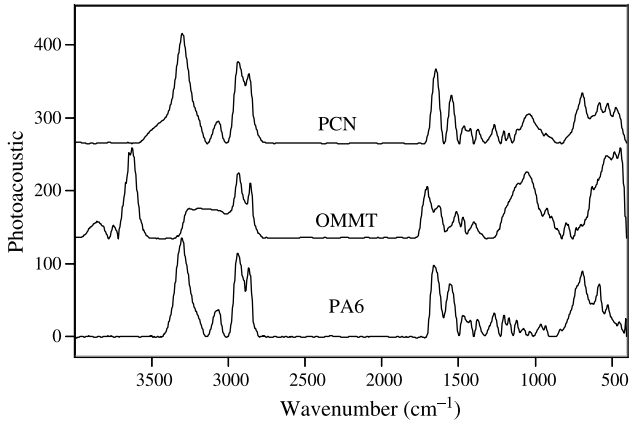

Fig. 11. Photoacoustic FTIR spectra of PCN, OMMT, and PA6 in the energy range of 4000–400 cm^{-1} at scan speed of 0.15 cm^{-1}.

Table 2
Band assignments of photoacoustic FTIR spectra of polyamide6 (PA6) and polymer clay nanocomposite (PCN)

Sample	Wave number range (cm^{-1})	Bands	Refs.
PA6			
	3300	N–H bound stretching	[12,26,30,
	3069	Fermi resonance of N–H stretching	59,61–64]
	2935	C–H asymmetric stretching	
	2867	C–H symmetric stretching	
	1658	Amide I	
	1548	Amide II	
	1469–1418	CH_2 scissoring	
	1372, 1266	Amide III and CH_2 wagging	
	1203	CH_2 twisting or wagging	
	1123–1076	C–C stretching	
	958–833	Skeletal vibration	
	730	CH_2 rocking	
	691	Amide V	
	579–447	Amide VI vibration band	
PCN			
	3298	Hydrogen bonded N–H stretching	[12,25,26, 29,30,51–
	3065	Fermi resonance of N–H stretching	54,56,57, 59,63–67]
	2934	C–H asymmetric stretching	
	2867	C–H symmetric stretching	
	1642	Amide I	
	1543	Amide II	
	1462–1419	CH_2 deformation	
	1370	Amide III and CH_2 wagging	
	1264	Amide III and CH_2 wagging	
	1201	Amide III and CH_2 wagging	
	1168	CH_2 twist/wagging	
	1120, 1059, 1028	Si–O in-plane stretching	
	959	Si–OH vibration	
	927	CO–NH in plane vibration	
	886	Al–FeOH deformation	
	847–836	Al–MgOH deformation	
	799	Si–O stretching of quartz and silica	
	690	Amide V	
	578–469	Amide VI vibration band	

octahedral layer in MMT structures, which are given in details in Table 2.

In the Fig. 12, the PA FTIR spectra of PCN, PA6 and OMMT are shown in the range of 3700–2700 cm^{-1}. It is seen that the sharp O–H stretching band at 3645–3628 cm^{-1} and broad band of ionically bonded N–H stretching at 3256–3035 cm^{-1} of OMMT are completely absent in PCN. The position of C–H symmetric stretching band in PCN at 2867 cm^{-1} has shifted by 14 cm^{-1} into higher energy side with respect to its position in OMMT. Otherwise the position and shape of all the bands in this energy-region in both PA6 and PCN are almost identical.

The PA FTIR view of the spectra of PCN, PA6 and OMMT are shown in the Fig. 13 for the energy range of 1800–1300 cm^{-1}. The C=O band at 1713–1701 cm^{-1} and R–COO band at 1511 and 1396 cm^{-1} present in OMMT are not observed in PCN. The amide-I band at 1658 cm^{-1} in PA6 has

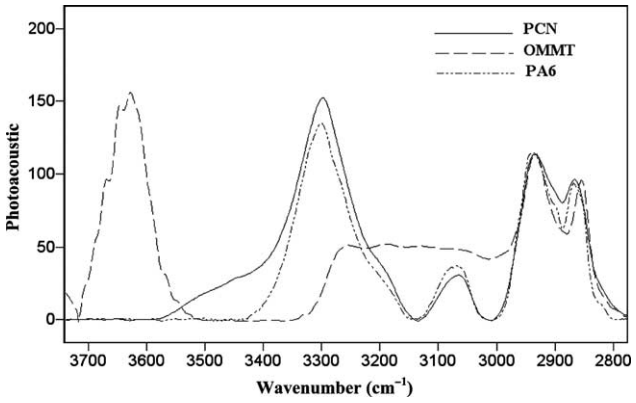

Fig. 12. Photoacoustic FTIR spectra of PCN, OMMT, and PA6 in the energy range of 3800–2750 cm^{-1} at scan speed of 0.15 cm^{-1}.

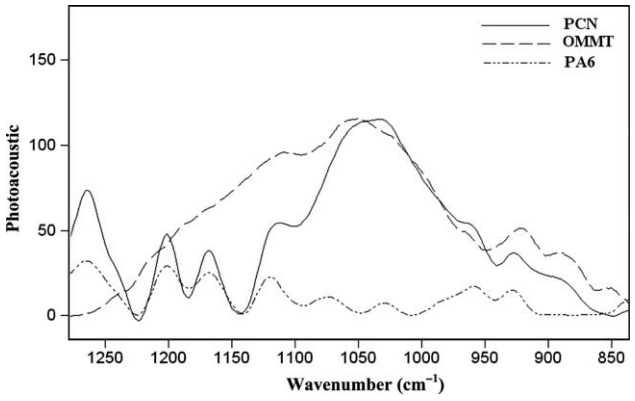

Fig. 14. Photoacoustic FTIR spectra of PCN, OMMT, and PA6 in the energy range of 1300–800 cm^{-1} at scan speed of 0.15 cm^{-1}.

shifted by 16 cm^{-1} to lower energy side with respect to that of PCN. The other shifting of bands at 1548 and 1462 cm^{-1} of PA6 compared to PCN are very small and close to the resolution of data acquisition of equipment (4 cm^{-1}) and hence may be neglected. In the energy range of 1300–800 cm^{-1}, the presence of Si–O band in the PCN and OMMT is very prominent as shown in Fig. 14.

The deconvoluted spectra of PCN, OMMT and MMT are provided in Fig. 15 for detailed band assignment and comparison of bands in the Si–O region. From Fig. 15, it is evidenced that the Si–O out-of-plane stretching band in PCN is absent as observed in OMMT. Furthermore the Si–O in-plane stretching band at 1120 and 1028 cm^{-1} in PCN has shifted to lower energy side by 8 and 6 cm^{-1}, respectively, with respect to their positions in OMMT.

3.5. Discussion of FTIR results of polyamide 6 (PA6), OMMT and PCN

The ionic bonded N–H band, which was found in OMMT in Fig. 5, is not seen in PCN as seen in Fig. 12. The N–H band region of PCN is almost similar to that of PA6, which indicates that the band contribution from 12-aminolauric acid is not present in this energy range. The possible explanation for this may be that the tiny amount of 12-aminolauric acid, present in the OMMT, is not sufficient in amount to produce the clear band of modifier. Therefore contribution from spectra of 12-aminolauric acid is not prominent in the N–H region in PCN as seen in Fig. 12. In Fig. 16 the Si–O band region of PCN, OMMT and MMT are shown.

The Si–O bands in MMT occur at 1110–1025 cm^{-1}, and that occurs in PCN and OMMT at 1120–1028 cm^{-1} and 1112–1022 cm^{-1}, respectively. The Si–O out-of-plane stretching band is absent in PCN as well as in OMMT which is present prominently in MMT as seen from the Fig. 16. In Fig. 15 it is further observed that in MMT the broader band comes first followed by a shoulder in Si–O region, where as in the Si–O region in both PCN and OMMT, the small shoulder appears before the broad sharp band and the shape of the bands are almost identical. Hence it is clearly seen that the nature, shape and position of peaks in Si–O region of PCN is much more close to OMMT than that of MMT, which indicates that the modifier is still present in PCN, otherwise the peaks in Si–O region of PCN would have been similar to MMT rather than OMMT.

Fig. 15 exhibits that the Si–O band in PCN has shifted compared to that of OMMT in two positions by 8 and 6 cm^{-1}.

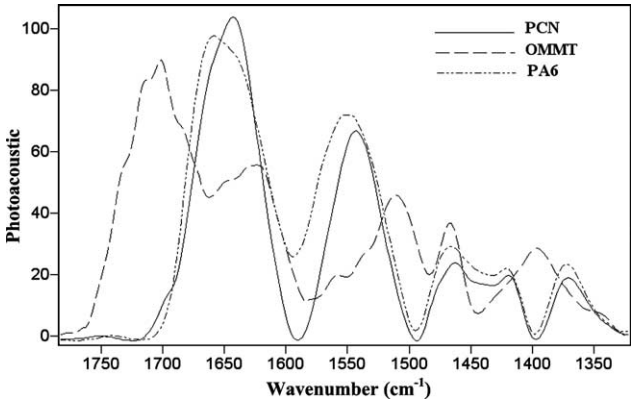

Fig. 13. Photoacoustic FTIR spectra of PCN, OMMT, and PA6 in the energy range of 1800–1300 cm^{-1} at scan speed of 0.15 cm^{-1}.

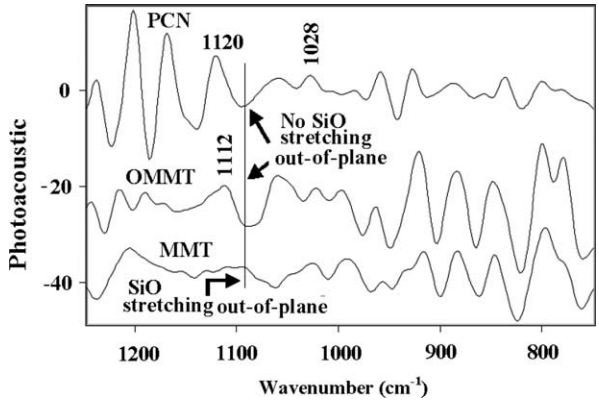

Fig. 15. Double derivative of Photoacoustic FTIR spectra of PCN, OMMT, and MMT in the energy range of 1300–750 cm^{-1} at scan speed of 0.15 cm^{-1}.

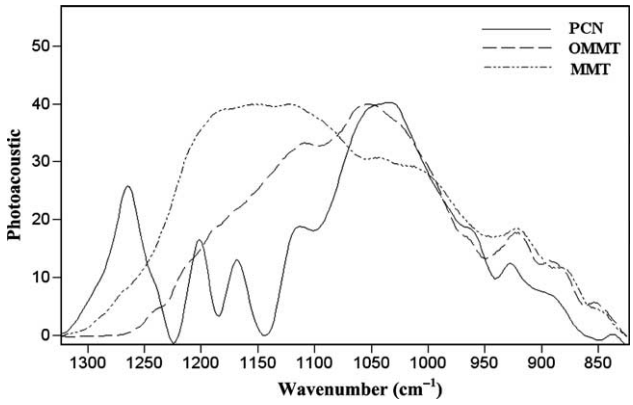

Fig. 16. Photoacoustic FTIR spectra of PCN, OMMT, and MMT in the energy range of 1350–800 cm^{-1} at scan speed of 0.15 cm^{-1}.

The hydrogen of amine group present in PA6 possibly forms the hydrogen bond with COOH group of 12-aminolauric acid, which is already bonded with silica tetrahedral of MMT or directly with the lone pair of surface oxygen present in silica tetrahedra of montmorillonite. This bonding of PA6 with silica tetrahedral oxygen may have caused shifting of Si–O longitudinal stretching band and Si–O stretching band in PCN with respect to OMMT. The hydrogen bond formation of amine group of PA6 with surface oxygen of tetrahedral layer of silicon tetrahedra may cause the slight shifting of N–H stretching band in PCN with respect to pure PA6 as exhibited in the Fig. 12. Similarly the shifting of C–H symmetric band by 14 cm^{-1} in Fig. 12 may be attributed to the same hydrogen bond formation of amine group of PA6 with surface oxygen of silica tetrahedra or with carbonyl band of aminolauric acid; but this end tethering of long carbon chain is not sufficient enough to be the cause of huge shifting of C–H symmetric stretching vibration in PCN compared to PA6. From Fig. 12 it is also seen that OMMT has sharp O–H stretching band at 3645–3628 cm^{-1}, which is not seen in PCN. A reasonable explanation of this is not yet found and is being investigated.

In Fig. 13 the shift of amide-I band in PCN to the lower energy side with respect to PA6 is attributed to the formation of hydrogen band of amine group of PA6 with carbonyl group of aminolauric acid of OMMT or lone pair of surface oxygen of silicon tetrahedra of montmorillonite. The absence of C=O at 1713 and 1701 cm^{-1} in PCN appears to result of the failure of generating sufficient signal by tiny amount of modifier present in OMMT as stated earlier.

The organic modifier, 12-aminolauric acid is a highly polar organic compound because of the presence of NH_2 and COOH group. Formic acid (FA) is also strong polar organic solvent. Because of the close solubility parameters of the two, the FA can easily dissolve the 12-aminolauric acid. When the OMMT is added to the solution of dissolved PA6 and FA, the excess amount of FA present in the PA6-FA solution may have dissolved part of 12-aminolauric acid from the clay gallery of OMMT. This dissolution of 12-aminolauric acid may have caused slight decrease in *d*-spacing in PCN with respect to OMMT, which is also in agreement with the XRD result, where the reduction in *d*-spacing in PCN compared to OMMT has been found.

4. Conclusions

In this work, we have used PA FTIR, and MD simulation to evaluate the interactions between the clay, modifier and polymer, and the intercalation behavior of OMMT and PCN. We have used Na^+-MMT clay, PA6 polymer and 12-aminolauric acid as organic modifier. From these experiments and simulations, we report the following conclusions:

(I) The H–OH stretching band at 3486–3234 cm^{-1} in MMT disappears in the OMMT, which indicates the replacement of adsorbed interlayer water by intercalated organic modifier in the OMMT.

(II) Evolvement of C=O band at 1713–1701 cm^{-1} in OMMT indicates the protonation of COO– functional group of 12-aminolauric acid into COOH. Hydrogen bonded C–O band at 1466 cm^{-1} in OMMT indicates the formation of hydrogen bond between COOH end group of organic modifier and surface oxygen of silica tetrahedra present in the MMT clay sheet.

(III) Evolvement of broad ionic bonded stretching band in OMMT in the range of 3256–3035 cm^{-1} in place of sharp N–H stretching band in 12-aminolauric acid indicates the ionic interaction of NH_2 end group of 12-aminolauric acid with the surface oxygen of silica tetrahedra present in the interlayer clay space. The shift of N–H band in the OMMT compared to that of MMT also supports the phenomenon.

(IV) Shifting of Si–O in-plane stretching band in OMMT suggests formation of non-bonded interactions of surface oxygen lying on the interlayer silica tetrahedra of MMT with the end functional groups of organic modifier. The absence of Si–O out-of-plane stretching band in OMMT possibly indicates the changes in structural orientation of MMT by organic modifier.

(V) In the minimized MD model of OMMT, the orientation of intercalated organic modifier was found parallel to the interlayer clay surface. The functional end groups of organic modifier in the minimized OMMT model was found projected towards the clay surface. The alignment and distance of functional end groups of organic modifier from the interlayer silica tetrahedra layer indicates possible formation of non-bonded interaction of surface oxygen of MMT with the functional end groups of organic modifier, which is in agreement with the PA FTIR result.

(VI) The shifting of Si–O in-plane stretching band observed in PCN with respect to OMMT indicates the hydrogen bond formation of end-tethered organic modifier or surface oxygen of clay surface with the functional groups of polymer intercalated in the OMMT.

(VII) The shift in position by 16 cm^{-1} of amide-I band at 1462 cm^{-1} in PCN with respect to PA6 also indicates the formation of hydrogen bond between amide group

of PA6 and functional group of end-tethered organic modifier or surface oxygen of clay surface.

Acknowledgements

The authors would like to acknowledge the use of computational resources at Center for High Performance Computing (CHPC), NDSU and Biomedical Research Infrastructure Network (BRIN). We would like to thank Dr Gregory H. Wettstein for hardware and software support.

References

[1] Okada A, Kawasumi M, Usuki A, Kojima Y, Kurauchi T, Kamigaito O. Mater Res Soc Symp Proc 1990;171:45.
[2] Pinnavaia TJ, Lan T. Proc Am Soc Compos Tech Conference 1996;11: 558.
[3] Giannelis EP. Adv Mater 1996;8:29.
[4] Maity P, Yamada K, Okamoto M, Ueda K, Okamoto K. Chem Mater 2002;14:4656.
[5] Pramanik M, Srivastava SK, Biswas KS, Bhowmick AK. J Appl Polym Sci 2003;87:2216.
[6] Zhang G, Jiang C, Su C, Zhang H. J Appl Polym Sci 2003;89:3159.
[7] Wang D, Wilkie CA. Polym Degrad Stab 2003;80:171.
[8] Lim ST, Lee CH, Choi HJ, Jhon MS. J Polym Sci, Part B: Polym Phys 2003;41:2052.
[9] Park HM, Lee WK, Park CY, Cho WJ, Ha CS. J Mater Sci 2003;38:909.
[10] Chen GX, Hao GJ, Guo TY, Song MD, Zhang BH. J Mater Sci Lett 2002; 21:1587.
[11] Ma CCM, Kuo CT, Kuan HC, Chiang CL. J Appl Polym Sci 2003;88: 1686.
[12] Pramoda KP, Liu T, Liu Z, He C, Sue HJ. Polym Degrad Stab 2003;81:47.
[13] Wang S, Hu Y, Wang Z, Yong T, Chen Z, Fan W. Polym Degrad Stab 2003;80:157.
[14] Zhang J, Wilkie CA. Polym Degrad Stab 2003;80:163.
[15] Liu T, Lim KP, Tjiu WC, Pramoda KP, Chen ZK. Polymer 2003;44:3529.
[16] Kim TH, Lim ST, Lee CH, Choi HJ, Jhon MS. J Appl Polym Sci 2003;87: 2106.
[17] Priya L, Jog JP. J Polym Sci, Part B: Polym Phys 2003;41:31.
[18] Krikorian V, Kurian M, Galvin ME, Nowak AP, Deming TJ, Pochan DJ. J Polym Sci, Part B: Polym Phys 2002;40:2579.
[19] Xu M, Choi YS, Kim YK, Wang KH, Chung IJ. Polymer 2003;44:6387.
[20] Tang Y, Hu Y, Song L, Zong R, Gui Z, Chen Z, Fan W. Polym Degrad Stab 2003;82:127.
[21] Chang JH, Park DK. Polym Bull 2001;(47):191.
[22] Ray SS, Yamada K, Okamoto M, Ueda K. Nano Lett 2002;2(10):1093.
[23] Ray SS, Okamoto M. Prog Polym Sci 2003;28:1539.
[24] Chen TK, Tien YI, Wei KH. Polymer 2000;41:1345.
[25] Liang ZM, Yin J, Xu HJ. Polymer 2003;44:1391.
[26] Wu Q, Liu X, Berglund LA. Polymer 2002;43:2445.
[27] Sohn JR, Kim JT. Langmuir 2000;16:5430.
[28] Sohn JR, Lee SI. Langmuir 2000;16:5024.
[29] Wan C, Zhang Y, Zhang Y. Polym Test 2004;23:299.
[30] Zhang G, Li Y, Yan D. J Polym Sci, Part B: Polym Phys 2004;42:253.
[31] Wang M, Zhao F, Guo Z, Dong S. Electrochim Acta 2004;49:3595.
[32] Katti DR, Schmidt S, Ghosh P, Katti KS. Clays Clay Miner 2005;53(2): 171.
[33] Schmidt S, Katti DR, Ghosh P, Katti K. Langmuir 2005;21:8069.
[34] Katti DR, Ghosh P, Schmidt S, Katti KS. Biomacromolecules; 2005; 6: 3276.
[35] Greenwell HC, Harvey HJ, Boulet P, Bowden AA, Coveney PV, Whiting A. Macromolecules 2005;38:6189.
[36] Sinsawat A, Anderson KL, Vaia RA, Farmer BL. J Polym Sci, Part B: Polym Phys 2003;41:3272.
[37] Swenson J, Smalley MV, Hatharasinghe HLM, Fragneto G. Langmuir 2001;17:3818.
[38] Boulet P, Coveney PV, Stackhouse S. Chem Phys Lett 2004;389:261.
[39] Muller R, Hrobarikova J, Calberg C, Jerome R, Grandjean J. Langmuir 2004;20:2982.
[40] Sheng N, Boyce MC, Parks DM, Rutledge GC, Abes JI, Cohen RE. Polymer 2004;45:487.
[41] Bohning M, Goering H, Fritz A, Brzezinka KW, Turky G, Schonhals A, et al. Macromolecules 2005;38:2764.
[42] Tanaka G, Goettler LA. Polymer 2003;43:541.
[43] Zeng QH, Yu AB, Lu GQ, Standish RK. Chem Mater 2003;15:4732.
[44] Minisini B, Tsobnang F. Compos Part A 2005;36:531.
[45] Shah K, Chiu P, Jain M, Fortes J, Moudgil B, Sinnott S. Langmuir 2005; 21:5337.
[46] Zeng QH, Yu AB, Lu GQ, Standish RK. J Phys Chem B 2004;108:10025.
[47] Hackett E, Manias E, Giannelis EP. J Chem Phys 1998;108(17):7410.
[48] Skipper NT, Sposito G, Chang FR. Clays Clay Miner 1995;43:285.
[49] Skipper NT, Chang FR, Sposito G. Clays Clay Miner 1995;43:294.
[50] Rosencwaig A. Photoacoustics and photoacoustic spectroscopy. New York: Wiley; 1980.
[51] Yan L, Roth CB, Low PF. Langmuir 1996;12:4421.
[52] Madejova J. Vib Spectro 2003;31:1.
[53] Magaraphan R, Lilayuthalert W, Sirivat A, Schwank JW. Compos Sci Tech 2001;61:1253.
[54] Zhu Y, Sun DX. J Appl Polym Sci 2004;92:2013.
[55] Liu W, Ni Y, Xiao H. J Colloid Interface Sci 2004;275:584.
[56] Madejova J, Komadel P. Clays Clay Miner 2001;49(5):410.
[57] Hsueh HB, Chen CY. Polymer 2000;44:5275.
[58] Yu YH, Yeh JM, Liou SJ, Chen CL, Liaw DJ, Lu HY. J Appl Polym Sci 2004;92:3753.
[59] Silverstein RM, Webster FX. Spectrometric identification of organic compounds. New York: Wiley; 1998.
[60] Sadhu S, Bhowmick AK. J Appl Polym Sci 2004;92:678.
[61] Schmidt P, Schneider B, Cefelin P. J Polym Sci, Part C 1967;16:229.
[62] Loo LS, Gleason KK. Macromolecules 2003;36:2587.
[63] Schneider B, Schmidt P, Wichterle O. Institue of macromolecular chemistry, Czechoslovak academy of science, Pargue. vol. 27 1952 p. 1749.
[64] Chen G, Shen D, Feng M, Yang M. Macromol Rapid Commun 2004;25: 1121.
[65] Hallam HE, Jones CM. J Mol Struct 1967;68(1):425.
[66] Yeh JM, Liou SJ, Chang YW. J Appl Polym Sci 2004;91:3489.
[67] Viville P, Lazzaroni R, Pollet E, Alexandre M, Dubois P, Borcia G, et al. Langmuir 2003;19:9425.